Microkinetic Model for the Pyrolysis of Methyl Esters: From Model Compound to Industrial Biodiesel

Ruben De Bruycker, Steven P. Pyl, Marie-Françoise Reyniers, Kevin M. Van Geem, and Guy B. Marin
Laboratory for Chemical Technology, Ghent University, Technologiepark 914, 9052 Gent, Belgium

DOI 10.1002/aic.14953
Published online July 24, 2015 in Wiley Online Library (wileyonlinelibrary.com)

A tool for the generation of decomposition schemes of large molecules has been developed. These decomposition schemes contain radicals which can be eliminated from the model equations if both the μ-hypothesis and the pseudosteady-state approximation are valid. The reaction rate coefficients and thermodynamic parameters have been calculated by incorporating a comprehensive group additive framework. A microkinetic model for the pyrolysis of methyl esters with a carbon number of up to 19 has been generated using this tool. It is validated by comparing calculated and experimental yields of the pyrolysis of methyl decanoate and novel rapeseed methyl ester pyrolysis data in the temperature range from 800 to 1100 K and methyl ester partial pressure range from 1×10^{-3} to 1×10^{-2} MPa. This modeling frame work allows to not only assess the use of methyl ester mixtures as potential feedstock for olefin production but also their effect as blend-in or trace impurity. © 2015 American Institute of Chemical Engineers *AIChE J*, 61: 4309–4322, 2015

Keywords: pyrolysis, methyl esters, kinetic modeling, group additivity, C=C double bond

Introduction

Pyrolysis of alkanes, cycloalkanes, alkenes, aromatics, alcohols, and methyl esters, mainly proceeds through a free-radical mechanism.[1,2] This process is characterized by a vast number of species and reactions which increases dramatically with the molecular mass of the feed.[1,3] Developing microkinetic models which describe the thermal decomposition of large molecules thus requires the use of automatic reaction network generation software. Most of these tools require the input of the feed as well as a set of reaction families. The reaction generator subsequently matches molecules and reaction families to add new reactions and molecules to the reaction network. Examples of such tools are Genesys,[4] RING,[5] RMG,[6] EXGAS,[7] NETGEN,[8,9] REACTION.[10] The output of these network generators is generally a CHEMKIN readable file containing thermodynamic data, derived from the group additivity method originally developed by Benson,[11] and elementary reactions, with kinetic parameters often derived from rate rules such as the Evans–Polanyi relationship.[12] Despite being general, the aforementioned tools require constrains to limit the number of species and reactions. Thus, automated reaction network generation has mainly been used for relatively small molecules.

The need for reaction networks of heavy feeds will, however, increase. Notable examples are the steam cracking of vacuum gas oils and the fast pyrolysis of biomass. MAMA[1] is a reaction network generator that has been used to create kinetic models for molecules with a high molecular mass. This program decomposes large radicals, for example, formed by hydrogen abstraction of large molecules, until a distribution of primary products remains. The obtained product spectrum is retained in such reactions, rather than the large radical itself. MAMA makes use of a library of kinetic parameters and the temperature dependence of the stoichiometric coefficients of the various products in the final equivalent reactions is neglected.

In this work, a new automated network generation code is presented called PRIM-O, based on the earlier version called PRIM,[13] that can be used for large hydrocarbons, large oxygen-containing compounds, and mixtures thereof. The main differences compared to previous version is (1) the use of group additivity for both kinetics and thermodynamics, based on the work by Benson,[11] and (2) the extension toward oxygenated components.

The pyrolysis of methyl esters has been chosen to assess its capabilities and limitations. Methyl esters have received a lot of interest in the past few decades given their potential to be a sustainable alternative to fossil fuels. Engine studies showed that these oxygenated fuels have the tendency to reduce soot formation[14–16] but result in increased NO_x formation compared to traditional diesel fuels.[15,17–19] Methyl esters are generally produced through the transesterfication of vegetable oils with methanol[20,21] which can be used as an alternative feedstock for olefin production.[22–25]

A kinetic model for the thermal decomposition of methyl esters has been generated. In order to validate this model, experimental pyrolysis data with detailed product distribution is required. To the best of our knowledge, such data is currently unavailable for real rapeseed methyl ester (RME)

Additional Supporting Information may be found in the online version of this article.

Correspondence concerning this article should be addressed to K. M. Van Geem at kevin.vangeem@ugent.be

mixtures. Therefore, pyrolysis experiments have been performed using a continuous flow tubular reactor setup with dedicated online analysis section for product identification and quantification. Furthermore, commonly used assumptions such as the μ-hypothesis[26] and the pseudosteady-state approximation[27–29] (PSSA), also known as the quasisteady-state-approximation, are verified.

Experimental

The experimental reactor setup has been described in detail elsewhere,[30–32] and therefore, only a brief description based on Djokic et al.[31] and Pyl et al.[32] will be given here. A schematic overview of the experimental setup is given in the Supporting Information.

The RME feed was provided by CARGILL[33] and was used without further treatment. The mixture comprises methyl esters with alkyl chains up to 24 carbon atoms and up to 3 double bonds. The major constituents are methyl palmitate (21 mol %), methyl stearate (2.5 mol %), methyl oleate (53 mol %), methyl linoeate (15 mol %), and methyl linolenate (5 mol %). A detailed composition can be found in Supporting Information. The (liquid) methyl ester feedstock was fed using a mass flow controlled pump (LIQUI-FLOW Bronkhorst) into a vaporizer. The mass flow of the diluent, that is, nitrogen (Air Liquide, purity + 99.999 mol %), was controlled using a Coriolis mass flow controller (CORI-FLOW Bronkhorst). A heated quartz pellet-filled mixer upstream of the reactor ensures a homogeneous nitrogen—methyl ester gas mixture.

This mixture enters a 1.475-m-long reactor with an internal diameter of 6 mm made out of Incoloy 800HT. The reactor is placed vertically in an electrically heated rectangular furnace and the pressure is kept constant by a valve downstream of the reactor. In all experiments, the reactor is operated nearly isothermally with a steep temperature increase at the inlet and a steep temperature drop at the reactor outlet. Eight thermocouples along the reactor monitor the process gas temperature at different positions. The measured temperature profiles are provided in Supporting Information. Two manometers, positioned at the inlet and outlet of the reactor, record the coil inlet pressure and the coil outlet pressure, respectively. The pressure drop over the reactor was found to be negligible.

The analysis section of the pyrolysis setup has been discussed previously.[32] In short, it consists of several dedicated gas chromatographs, that is, a refinery gas analyzer (RGA), a light oxygenates analyzer (LOA) and a two-dimensional (2-D)-gas chromatograph (GC×GC) equipped with a flame ionization detector (FID) and time of flight mass spectrometer (TOF-MS). The RGA quantifies hydrogen and other permanent gases using two thermal conductivity detectors (TCD) and the C_{4-} hydrocarbon fraction using a FID. Nitrogen, the diluent used in this work, was used as primary internal standard. The LOA detects small oxygenates such as formaldehyde, methanol, and water using a TCD. Propene was used as secondary internal standard for this chromatogram. The GC×GC is able to identify (TOF-MS) and quantify (FID) the complete effluent stream ranging from methane to pyrene. Methane was used as secondary internal standard. For each studied condition, at least three repeat analyses were performed. For all runs, the mass balances were within the range of 95–105%. Deviations are attributed to uncertainties in the mass flow rates of the feed and the internal standard (N_2). After normalization of the total mass balance, elemental balances (C, H, O) were verified. The estimated experimental error of the measured product yields is 5% rel. in line with previous work.[31] The experimental error is lower for components with higher mole fractions.

Modeling Methodology

Radicals, formed during the pyrolysis of methyl esters, can react further through various channels such as β-scission, intermolecular/intramolecular hydrogen abstraction, and intermolecular/intramolecular radical addition. As long as the feed molecules are sufficiently small, it is possible to account for each individual reaction, which leads to an accurate kinetic model. A higher number of heavy atoms, that is, nonhydrogen atom, in the feed molecules leads to a dramatic increase in species and reactions.[8,34,35] The strategies followed to overcome the aforementioned issue will be discussed in the subsequent sections.

In line with earlier work,[13,34,36–38] the kinetic network has been split up into two subnetworks, that is, a β-network containing all thermodynamic and kinetic data of small molecules (typically C_{5-}), and a μ-network containing decomposition schemes for larger molecules (typically C_{6+}). The proposed separation originates from the μ-radical hypothesis,[26] which proposes that radicals with a high number of heavy atoms primarily react via monomolecular reactions, μ-reactions, while bimolecular reactions, β-reactions, can be neglected.

Every reaction which forms a μ-radical is present in the μ-network. These μ-radicals react by intramolecular hydrogen abstraction and β-scission, that is, monomolecular reactions, until only nonradical species and C_{5-} radicals remain. Rather than incorporating the μ-radicals explicitly in the μ-network, they can be substituted by their decomposition product spectrum. This is possible by combining the μ-radical hypothesis with the PSSA.[13] Reactions in the μ-network are collections of elementary reactions appearing as an equivalent single-step reaction.[1,13,39]

In the following paragraphs, the various parts of the kinetic model are discussed in detail. First, the origin of the β-network is discussed. This is followed by details regarding the generation of the μ-network using PRIM-O. Special attention is dedicated to validation of the μ-hypothesis and PSSA for ester radicals. Finally, the coupling of the complete kinetic model with CHEMKIN, a software tool for solving complex chemical kinetics problems, is discussed. The kinetic model can be found in Supporting Information.

β-*network*

The β-network mainly contains thermodynamic data of small molecules (C_{5-}) and an appropriate set of elementary reactions. Three classes of molecules are present in the β-network, that is, nonradical species, radicals that are solely involved in bimolecular reactions (such as $H^{\bullet}$ and $CH_3^{\bullet}$) and radicals that are involved in mono and bimolecular reactions. In this work, the β-network describes thermal decomposition of methyl butanoate (MB), pyrolysis of C_{5-} hydrocarbons, reactions of small oxygenates and polycyclic aromatic hydrocarbon (PAH) formation through cyclopentadienyl chemistry.

The primary decomposition reactions of MB were taken from an ab initio study by Huynh and Violi.[40] Their results were successfully applied to predict ignition delays as well as the formation of CO, CO_2, CH_3, and C_2H_4 during MB pyrolysis in a shock tube.[41–43]

A hydrocarbon pyrolysis mechanism developed by Sabbe et al.[44] and validated for steam cracking of small alkanes was

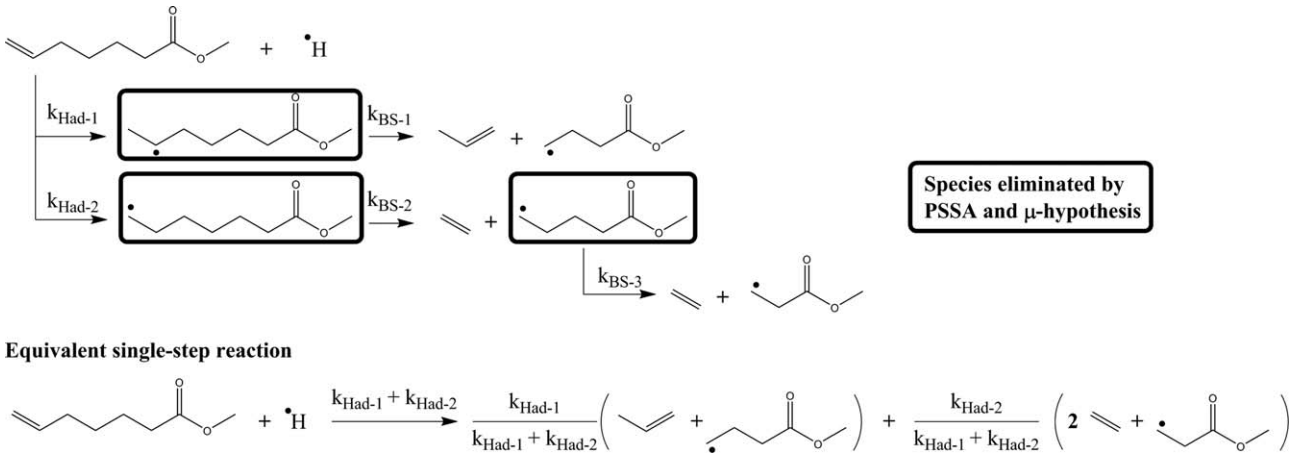

Figure 1. Hydrogen addition on methyl hept-6-enoate and subsequent decomposition reactions.

The equivalent single-step reaction is obtained after elimination of the concentration of the μ-radicals, that is, methyl heptanoate-6-yl, methyl heptanoate-7-yl, and methyl pentanoate-5-yl, considering all the elementary reactions using the pseudosteady-state approximation (PSSA).

also added to the β-network. The kinetics of the referred mechanism are obtained from the same CBS-QB3-based group additive models as applied in the μ-network, see subsequent paragraph. Thermodynamic data were determined using accurate quantum chemical CBS-QB3 calculations.

Reactions and thermochemistry of small oxygenated species were taken from the mechanism by Li et al.,[45] which includes decomposition of formaldehyde and methanol. While this reaction network was developed for combustion, it has been validated for pyrolysis conditions as well.[45]

Finally, reaction paths for formation of PAH through cyclopentadienyl radicals were based on the work of Cavallotti et al.[46,47]

Generation of the μ-network using PRIM-O

Each reaction in the μ-network was generated using PRIM-O. As input, PRIM-O requires the structure of the molecule and the desired reaction. The algorithm searches for possible reactive moieties corresponding to that specific reaction and calculates the kinetic parameters associated with each elementary step. Subsequently, μ-radicals are identified. For these species, all possible monomolecular reaction routes are generated, for example, β-scission, intramolecular hydrogen abstraction, intramolecular radical addition. PRIM-O reiterates this procedure until all generated μ-radicals have decomposition paths. Finally, the μ-radicals can be eliminated from the model equations using the PSSA.[48] The μ-radicals are replaced by their complex product spectrum, comprising of nonradical species and small (C_{5-}) radicals, which leads to the so-called equivalent single-step reactions. All feed molecules and accompanying C_{6+} products were given as input to PRIM-O together with the possible reaction types, for example, hydrogen abstraction scission, radical addition.

As example, the hydrogen addition on methyl hept-6-enoate and its subsequent decomposition in PRIM-O is presented in Figure 1. Intramolecular hydrogen abstraction and hydrogen-centered β-scission are not included to reduce the complexity of the figure. Two possible reactive centra are recognized forming methyl heptanoate-6-yl and methyl heptanoate-7-yl. For both radicals, bimolecular reactions can be neglected and they are further decomposed in PRIM-O. Methyl heptanoate-6-yl reacts with formation of propene and MB-4-yl. The latter radical is assumed to be the largest radical for which bimolecular reactions cannot be neglected, hence, it is not further decomposed. Methyl heptanoate-7-yl forms ethene and methyl pentanoate-5-yl. The latter radical is a μ-radical and reacts further through carbon centered β-scission forming methyl propanoate-3-yl and, again, ethene. The complete hydrogen addition can be written as an equivalent single-step reaction where the stoichiometric coefficients are a function of the kinetic parameters of the various elementary steps. Note that the stoichiometric coefficients are temperature dependent and reflect the importance of the reaction path(s) leading to that specific species. In the presented example, these are function of the ratio of the kinetic parameters of both possible hydrogen additions. Hence, if a certain reaction path is favored, this will lead to a higher stoichiometric coefficient for the resulting species.

The validity of the μ-hypothesis and the PSSA will be assessed in the next paragraph. Subsequently, the calculation of kinetic and thermodynamic parameters in PRIM-O is discussed.

Network reduction strategies

Validation of the μ-Hypothesis. The μ-hypothesis[26] is a common assumption used to model pyrolysis and steam cracking of hydrocarbons.[34] This assumption allows to drastically reduce the number of differential equations that need to be solved without losing accuracy. The latter is of particular importance if these detailed kinetic models need to be applied in Computational Fluid Dynamics simulation.[49,50] Bimolecular reactions can be neglected when aliphatic radicals have more than five carbon atoms.[6,13,48] Given the alkyl chain in esters, the μ-hypothesis may be used for methyl ester-derived radicals.

To test this assumption and evaluate the effect of the presence of the ester function, a detailed kinetic model for thermal decomposition of methyl decanoate (MD), a moderately large methyl ester, has been constructed using Genesys.[4] Genesys uses group additivity models to estimate thermodynamic and kinetic data. The C_{6+} part of this mechanism is not a set of equivalent single-step reactions which would be the case if it would be generated by PRIM-O but, instead, all large radicals and all elementary reactions are explicitly taken into account. Furthermore, the C_{6+} part of the Genesys-generated mechanism contains several reactions which are neglected in the μ-

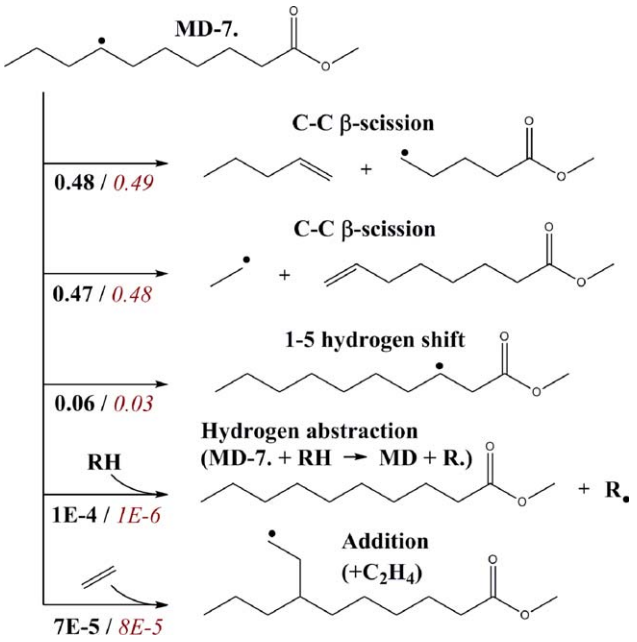

Figure 2. Possible consumption reactions for the μ-radical MD-7•.

Numbers indicate the relative contribution of the corresponding reaction path to the total consumption of MD-7• at 873 K (bold—black) and1073 K (italic—red), which were calculated with CHEMKIN using the plug flow reactor model and the Genesys-generated model, with $d_t = 6 \times 10^{-3}$ m, $z = 2 \times 10^{-2}$ m, $P = 0.1$ MPa, $F^0_{MD} = 5.4 \times 10^{-4}$ mol/s. [Color figure can be viewed in the online issue, which is available at wileyonlinelibrary.com.]

network generated using PRIM-O, for example, hydrogen abstraction by large radicals, addition of small olefins on MD radicals. The Genesys-generated mechanism comprises of 446 species and 2272 reactions and can be used to validate the μ-hypothesis by analyzing the fate of large radicals.

For example, in Figure 2, the various possible reaction routes of a MD radical and the corresponding relative consumption rates, calculated using the Genesys-generated mechanism, are presented. Note that the naming of radicals in this work reflect the name of the corresponding molecule and the position of the unpaired electron. The label of the radical position is consistent with the work by Fisher et al.,[51] that is, "M" if the radical is on the primary carbon atom of the methyl ester group, "2" if the radical is on the carbon α to the ester group, "3" if the radical is on the carbon β to the ester group, and so forth. Reaction paths of the radical can be divided in two groups, that is, monomolecular and bimolecular reactions. Under the operating conditions investigated in this work,[52,53] monomolecular reactions such as intramolecular hydrogen abstraction and β-scission reactions comprise the vast majority of the MD-7• consumption. Bimolecular reactions, for example, addition of small olefins on MD-7• and hydrogen abstraction of MD-7• forming MD, are negligible over the entire temperature range. MD-7• can thus be considered a μ-radical and the use of PRIM-O is justified for this species.

The μ-hypothesis has been tested for alkyl and ester radicals in the reaction system. The decomposition of MD radicals leads to formation of primary alkyl and methyl ester radicals. Hence, the following discussion will be restricted to these species.

The ratio of monomolecular reaction rate divided by bimolecular reaction rate as a function of carbon atoms for primary alkyl and methyl ester radicals, calculated using the Genesys-generated model, is presented in Figure 3. Reaction conditions correspond to the most severe conditions for the validity of the μ-hypothesis, that is, undiluted and low temperature. High radical partial pressures increase the importance of bimolecular reactions. Unimolecular radical reactions, such as C—C β-scission, often have higher activation energies compared to bimolecular radical reactions, such as hydrogen abstraction, see Table 2. Hence, the former are more affected by a decrease in temperature.[64] Note that only radicals containing three or more carbon atoms are displayed in Figure 3. Methyl and hydrogen radicals are only involved in bimolecular reactions. The ethyl radical cannot decompose through carbon centered β-scission compared to the other molecules displayed. As such, ethyl follows a different trend regarding μ to β reaction rate ratio. Ethyl has a μ to β reaction ratio of approximately 5 at the operation conditions of Figure 3.

Overall, small ester radicals appear to have a lower μ to β reaction ratio than alkyl radicals with the same number of carbon atoms. Obviously, their reactivity is influenced by the change in bond dissociation energies due to the ester functionality compared to alkyl radicals.[65] The most important bimolecular reaction for the *n*-alkyl and ester radicals is hydrogen abstraction from the feed molecule, that is, MD in the case of Figure 3.

A methyl ethanoate (ME) radical with the radical on the 2 position (ME-2•) is resonantly stabilized causing the rates of possible monomolecular reactions, that is, decomposition forming ketene plus methoxy and hydrogen shift to ME-M•, to be lower compared to decomposition of 1-propyl to ethene and methyl.[61]

A methyl propanoate (MP) radical with a radical on the 3 position (MP-3•) will decompose forming ethene and a methoxy-carbonyl radical. The rate of the latter C—C β-

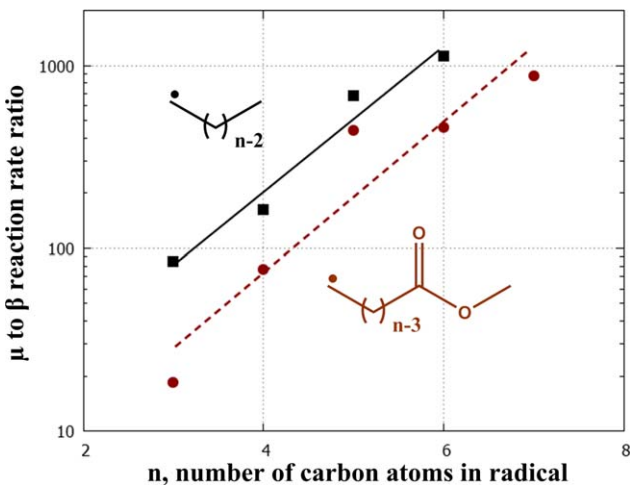

Figure 3. Calculated μ to β reaction rate ratio as a function of the number of carbon atoms in the radical: ■—primary *n*-alkyl radicals; ●—primary methyl ester radicals; lines, observed trend.

Reaction rates were calculated with CHEMKIN using the plug flow reactor model and the Genesys-generated model, with $d_t = 6 \times 10^{-3}$ m, $z = 2 \times 10^{-2}$ m, $P = 0.1$ MPa, $T = 873$ K, $F^0_{MD} = 5.4 \times 10^{-4}$ mol/s. [Color figure can be viewed in the online issue, which is available at wileyonlinelibrary.com.]

Table 1. Relative Error when Applying the Pseudosteady-State Approximation and the Chemical Lifetime for a Selection of Radicals

	873 K		1073 K	
	Lifetime (s)	$\lvert\Delta c_i^s/c_i\rvert$	Lifetime (s)	$\lvert\Delta c_i^s/c_i\rvert$
CH_3•	1.94×10^{-6}	1.47×10^{-5}	2.81×10^{-8}	1.53×10^{-4}
H•	6.95×10^{-9}	4.15×10^{-7}	5.71×10^{-10}	1.97×10^{-4}
MD-M•	1.70×10^{-6}	-2.54×10^{-6}	7.58×10^{-8}	-3.11×10^{-4}
MD-8•	6.04×10^{-8}	-2.86×10^{-6}	4.73×10^{-9}	-3.63×10^{-4}
MD-3•	5.97×10^{-8}	-2.65×10^{-6}	4.68×10^{-9}	-3.59×10^{-4}
MD-2•	5.50×10^{-8}	-3.87×10^{-7}	8.71×10^{-9}	-9.82×10^{-5}
MD-9•	5.06×10^{-8}	-1.90×10^{-6}	5.10×10^{-9}	-3.25×10^{-4}
MD-7•	5.00×10^{-8}	-1.72×10^{-6}	3.71×10^{-9}	-2.84×10^{-4}
MD-4•	3.89×10^{-8}	-2.09×10^{-6}	2.77×10^{-9}	-3.39×10^{-4}
MD-5•	2.49×10^{-8}	-8.40×10^{-7}	2.93×10^{-9}	-1.97×10^{-4}
MD-6•	7.41×10^{-9}	1.18×10^{-8}	1.94×10^{-9}	-1.15×10^{-4}
MD-10•	7.33×10^{-9}	-7.74×10^{-7}	1.18×10^{-9}	-2.18×10^{-4}

Reaction simulations were performed with CHEMKIN using the plug flow reactor model and the Genesys-generated model with $d_t = 6 \times 10^{-3}$ m, $z = 2 \times 10^{-2}$m, $P = 0.1$ MPa, $F_{MD}^0 = 4 \times 10^{-4}$ mol/s. Subsequently, KINALC, a CHEMKIN postprocessor, was used to calculate $\lvert\Delta c_i^s/c_i\rvert$ and the chemical life of each species i.

scission reaction is slower than the C—C β-scission of 1-butyl.[40,66]

Decomposition of the MB radical with a radical on the 4 position (MB-4•) will form ethene and ME-2•. As mentioned earlier, the latter species is resonantly stabilized and, thus, the rate of this C—C β-scission is higher than the rate of the C—C β-scission of 1-pentyl.[61] Note that 1-pentyl can isomerize to 2-pentyl through a favorable five-membered transition state, which is not possible in MB-4•. Both MB-4• and 1-pentyl have a comparable and high μ to β reaction rate ratio, $r_\mu/r_\beta \approx 500$. As, 1-pentyl radicals are commonly considered as the largest alkyl radicals with β-properties,[6] the largest ester radicals with β-properties are MB radicals in this work. The error introduced by neglecting bimolecular reaction for larger ester radicals can assumed to be negligible.

Validation of the PSSA. The second assumption is the PSSA. This has been used in various combustion, pyrolysis, and steam cracking models.[1,67–69] Since the kinetic network generated with PRIM-O makes use of the PSSA for μ-radicals, it is instructive to calculate the error that is introduced.

The pyrolysis of MD was simulated with the Genesys-generated network using CHEMKIN at two different temperatures, that is, 873 and 1073 K, and similar reactor conditions as Figure 2. Subsequently, KINALC,[27,67,70] a CHEMKIN postprocessor developed to analyze complex reaction mechanisms, is used to evaluate (1) the instantaneous error on the concentration of each species i when applying PSSA for this species, denoted as Δc_i^s, and (2) the chemical lifetime of each species i, defined as $c_i(z)/\sum_j \nu_{ij} r_j(z)$. Details regarding the procedure used in KINALC to calculate these properties can be found elsewhere.[67,70]

Table 1 presents the results for methyl, hydrogen, and radicals of MD (μ-radicals). Similar values were obtained for the other alkyl and ester radicals. The relative error on the concentration of a radical when applying the PSSA is found to be negligible, below 0.1%. The PSSA is valid for the pyrolysis of methyl esters and it is applied to μ-radicals in the PRIM-O network generation program. The μ-radicals can be eliminated from the model equations. This avoids the need to calculate their concentration during a reactor simulation, which gives rise to considerable speed-up.

The lifetime of the majority of MD radicals is as small as 10^{-9} s. MD with a radical on the methoxy group (MD-M•) has a lifetime which is about two orders of magnitude larger compared to the other MD radicals. The direct decomposition of this type of radical, with formation of formaldehyde and α-carbonyl radicals, is slower than C—C β-scission reactions which are the dominant reaction paths for the other MD radicals, explaining their longer lifetime.[40]

Kinetic data

In order to construct decomposition schemes for molecules present in the μ-network, on-the-fly calculation of rate coefficients for decomposition of molecules and (μ-) radicals is needed. In this work, rate coefficients are estimated using a comprehensive group additive data set, mainly derived by Sabbe and coworkers who applied Benson's group additivity concept to transition state theory.[60,71] Group additive values for radical decomposition reactions that are affected by the ester functionality were derived from the work by Huynh and Violi.[40]

In short, the applied group additive concept classifies possible reactions in so called elementary reaction families, see Table 2. Each reaction is characterized by a rate coefficient which depends on three parameters, that is, the activation energy E_a, the pre-exponential factor for each single-event $\tilde{A}$ and the number of single events n_e, that is, the number of energetically equivalent reaction paths from reactant(s) to transition state. The former two are calculated by taking the kinetic parameters of a reference reaction corresponding to the considered reaction family, $E_{a,ref}$ and $\tilde{A}_{ref}$, but adding contributions which take into account the difference in transition state between the considered reaction and the reference reaction, see Eqs. 1–3

$$k(T) = n_e \cdot \tilde{A} \cdot \exp\left(-\frac{E_a}{RT}\right) \tag{1}$$

$$E_a = E_{a,ref} + \sum_{i=1}^{n} \Delta GAV_{E_{a,i}}^0 \tag{2}$$

$$\log(\tilde{A}) = \log(\tilde{A}_{ref}) + \sum_{i=1}^{n} \Delta GAV_{\tilde{A},i}^0 \tag{3}$$

Thermodynamic data

The thermodynamic data for μ-species were determined based on Benson's group additivity method.[11] Various groups have made use of this technique which led to the development

Table 2. Kinetic Data in μ-Network

Reaction family	Reference Reaction	Log A_{ref}	$E_{a,ref}$	Ref.
μ-radical formation				
Bond Scission				
C—C	n-$C_4H_{10} \rightarrow C_2H_5\bullet + C_2H_5\bullet$	16.7	345.5	54
C—H	$C_2H_6 \rightarrow C_2H_5\bullet + H\bullet$	16.0	417.8	55,56
C—O	CH_3-C(=O)-O-$CH_3 \rightarrow CH_3$-C(=O)-O$\bullet + CH_3\bullet$	15.1	429.9	52
Intermolecular hydrogen abstraction				
by C.	$CH_4 + CH_3\bullet \rightarrow CH_3\bullet + CH_4$	6.5	84.4	57,58
by H.	$CH_4 + H\bullet \rightarrow CH_3\bullet + H_2$	8.0	66.4	59
Intermolecular radical addition				
by C.	$C_2H_4 + CH_3\bullet \rightarrow C_3H_7-1\bullet$	6.0	43.1	60
by H.	$C_2H_4 + H\bullet \rightarrow C_2H_5\bullet$	7.7	18.5	61
μ-radical decomposition				
β-scission				
C—C	$C_3H_7-1\bullet \rightarrow C_2H_4 + CH_3\bullet$	13.5	128.5	62
C—H	$C_2H_5\bullet \rightarrow C_2H_4 + H\bullet$	12.6	162.4	61
C—O	C_3H_7-C(=O)-O-$CH_2\bullet \rightarrow C_3H_7$-C(=O) $\bullet + CH_2O$	13.3	133.5	40
α-scission				
CO	C_3H_7-C(=O) $\bullet \rightarrow C_3H_7-1\bullet + CO$	13.5	71.8	40
Intramolecular hydrogen abstraction				
[1,4]	n-$C_4H_9-1\bullet \rightarrow n$-$C_4H_9-1\bullet$	11.0	86.2	54
[1,5]	n-$C_5H_{11}-1\bullet \rightarrow n$-$C_5H_{11}-1\bullet$	10.2	60.7	54
Intramolecular radical addition				
[1,5] endo	pent-1-en-5-yl → cyclopentyl	10.9	62.6	[x]
[1,5] exo	hex-1-en-6-yl → CH_3-cyclopentane	10.8	23.5	[x]
[1,6] endo	hex-1-en-6-yl → cyclohexyl	10.5	32.2	[x]
[1,6] exo	hept-1-en-7-yl → CH_3-cyclohexane	10.2	29.6	[x]
Concerted path reactions				
Retro-ene	1-$C_5H_{10} \rightarrow C_2H_4 + C_3H_6$	12.8	235.8	[x]
Acetate elimination	C_3H_7-C(=O)-O-$CH_3 \rightarrow CH_3$-C(=O)-O-$CH_3 + C_2H_4$	12.6	284.5	63

[x] Calculated using the methodology described in Refs. 57,60,61.

of independent, stand-alone programs such as THERGAS[72] and RMG's ThermoDataEstimator.[73] In this work, the thermodynamic data were generated in the NASA polynomial format using Genesys's ThermoGenerator[4] equipped with group additive values derived by Sabbe et al.[74] and Paraskevas et al.[75] from an extensive thermochemical database obtained by ab initio calculations at the CBS-QB3 level of theory.

Reactor model

Reactor simulations were performed using CHEMKIN-PRO.[76] Both the perfectly stirred reactor model and the ideal plug flow reactor model were used to model the respective datasets in this work. The plug flow assumption has been verified for the bench scale pyrolysis set up used in this work.[30,53] Since the constructed kinetic model is comprised of a μ-network, containing equivalent single-step reactions of which the stoichiometric coefficients are temperature dependent, and a β-network, containing reversible elementary reactions, the USRPROD routine was used to couple the kinetic model with the CHEMKIN framework. This option enables the user to define a subroutine that calculates the rate of production of all species for certain reactor conditions. Note that the kinetic model in Supporting Information can also be processed using OpenSMOKE++, an open-source software-tool for the simulation of reactors using detailed kinetic models, recently developed by Cuoci et al.[77] The USRPROD routine is available upon request.

Results and Discussion

Pyrolysis of MD

MD, having a medium-long length alkyl chain, is widely recognized as a good surrogate component for biodiesel. Both its combustion and pyrolysis characteristics have been studied thoroughly[52,53,78–80] and several extensive datasets regarding its thermal decomposition are available in literature.[52,53] In this work, the aforementioned experimental pyrolysis data is used to validate the μ-network generation algorithm and the applied rate rules.

Scission and hydrogen abstraction of MD causes μ-radicals to be formed and, thus, these reactions are generated with PRIM-O. The stoichiometric coefficients of the single-step equivalent hydrogen abstraction reaction of MD are displayed in Figure 4A for 873 and 1073 K. In this table, methyl esters with a carbon chain of length X with Y double bonds are denoted as CX:Y. A weak temperature dependence can be observed. The stoichiometric coefficient of the hydrogen radical has the largest relative increase, approximately doubling from 873 to 1073 K.

Hydrogen abstraction from the carbon atom α to the ester group is the favored hydrogen abstracting channel as this leads to a resonantly stabilized radical. Decomposition of this μ-radical leads to formation of methyl propenoate, the unsaturated methyl ester with the highest stoichiometric coefficient and, thus, selectivity, and a 1-heptyl radical, which in turn decomposes to ethene plus 1-pentyl. The selectivity towards C_{5+} 1-olefins and monounsaturated esters is fairly independent of the molecule's chain length. These molecules are formed by the various possible hydrogen abstractions along the alkyl chain of MD followed by carbon centered β-scission. As the reaction paths for the production of these unsaturated molecules occur in a similar hydrocarbon moiety, the corresponding reaction rate coefficients, and as such the stoichiometric coefficients, are comparable. Differences are encountered at the oxygenated end, that is, higher selectivity for octene since the "parent" radical MD-4• prefers this C—C β-scission due to formation of a resonantly stabilized ME radical, and at the alkyl end, that is, a lower selectivity for methyl

(A)

MD + R → RH + ∑ α_i(T) species$_i$					
species	α(873K)	α(1073K)	species	α(873K)	α(1073K)
H.	0,01	0,02	.C(=O)OCH$_3$	0,05	0,05
CH$_3$.	0,03	0,03	ME-2.	0,08	0,08
C$_2$H$_5$.	0,05	0,05	MP-3.	0,19	0,19
1-propyl	0,05	0,05	MB-4.	0,15	0,16
1-butyl	0,17	0,15	CO	0,03	0,08
1-pentyl	0,22	0,23	CH$_2$O	0,03	0,08
C$_2$H$_4$	0,77	0,82	C03:1	0,18	0,13
C$_3$H$_6$	0,10	0,10	C04:1	0,12	0,10
1-butene	0,07	0,06	C05:1	0,02	0,02
1-pentene	0,05	0,05	C06:1	0,05	0,05
1-hexene	0,05	0,05	C07:1	0,05	0,05
1-heptene	0,05	0,05	C08:1	0,05	0,05
1-octene	0,08	0,08	C09:1	0,03	0,03
1-nonene	0,05	0,05	C10:1	0,01	0,01

(B)

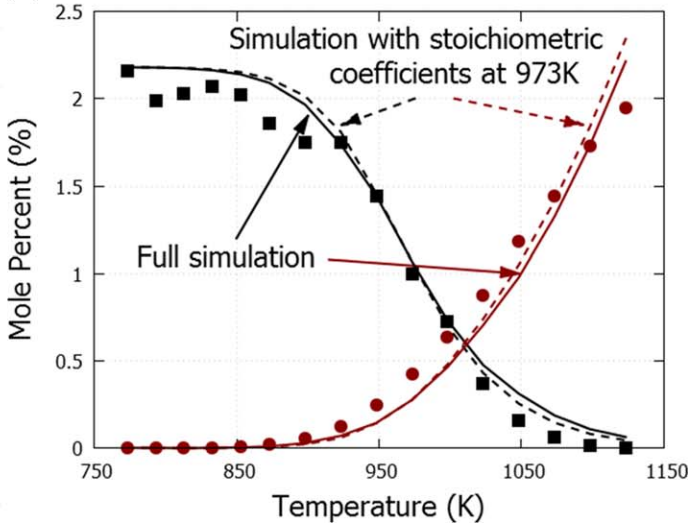

Figure 4. (A) Hydrogen abstraction reaction of methyl decanoate (MD). The stoichiometric coefficients α are obtained after elimination of the concentration of μ-radicals using the PSSA at 873 and 1073 K. (B) Mole fractions as a function of temperature for MD pyrolysis in a jet-stirred reactor[52]: ■—MD; ●—H_2; full lines, calculated with CHEMKIN using the perfectly stirred reactor model and the developed kinetic model; dashed lines, calculated with CHEMKIN using the perfectly stirred reactor model and a kinetic model where the stoichiometric coefficients of the equivalent single-step reactions were fixed to their values at 973 K.

[Color figure can be viewed in the online issue, which is available at wileyonlinelibrary.com.]

nonenoate since the "parent" radical MD-8• disfavors this C—C β-scission due to formation of a methyl radical.

Two extensive datasets for pyrolysis of MD are available in literature, one obtained by Herbinet et al.[52] in a jet-stirred reactor and one obtained by Pyl et al.[53] in a plug flow reactor. Both were used to test the performance of the kinetic model. Model performance for the latter dataset can be found in Supporting Information. In Figure 4B, experimental MD and hydrogen mole fraction profiles are compared to (1) the generated kinetic model and (2) a kinetic model where the temperature dependence of the stoichiometric coefficients of the reactions in the μ-network has been neglected and fixed to their values at 973 K, a selected intermediate temperature.

Fixing the stoichiometric coefficients at an intermediate temperature only has a minor effect on calculated results which is line with earlier observations for hydrocarbons.[39] Even for hydrogen, mainly formed by hydrogen abstraction of hydrogen radicals which experience the largest variation in stoichiometric coefficient, the difference is less than 10% at 1123 K. The MAMA program,[1,48] developed by Dente, Ranzi, and coworkers, neglects the temperature dependence of the stoichiometric coefficients, which proves to be a reasonable approximation under the conditions studied in this work. Throughout the rest of this work, calculations will be performed using the complete generated kinetic model.

Performance for other detected species is presented in Figure 5. The ester group decomposes with possible formation of CO and CO_2.[81] As discussed earlier, the relevant kinetic data for decomposition of the ester functionality was taken from the ab initio study by Huynh and Violi.[40] The model predicts the CO and CO_2 mole fraction profiles accurately and, thus, the rate rules derived from the referred work can assumed to be valid for the considered operating conditions.

The applied group additivity values describing the decomposition of hydrocarbons has been validated earlier.[44] Ethene, propene, and other olefins are formed from the alkyl chain in MD. As the model is able to capture the trend of all these species, the accuracy of these values is confirmed here as well. Note that propene has a low stoichiometric coefficient in the hydrogen abstraction reaction of MD, see Figure 4A. Retro-ene reactions of the olefins and unsaturated methyl esters, both having a double bond at the end of the carbon chain, are the main source of propene.[52]

Both experimental datasets comprise the yield of all esters and olefins with up to 10 carbon atoms. This allows to evaluate the product selectivities generated by the kinetic modeling algorithm. The yield of some unsaturated methyl esters, are displayed in Figure 5D. Methyl propenoate is the most abundantly formed ester and the effect of temperature on its mole fraction is captured well by the model. The experimental yield of methyl butenoate, the largest unsaturated methyl ester of which the decomposition is part of the β-network, matches the model prediction, only at the high temperatures, there appears to be a small over prediction. The applied rate rules can be assumed to be valid for MD pyrolysis and are extended to the pyrolysis of larger esters such as RME.

Pyrolysis of RME

Experimental Results. An experimental dataset regarding RME pyrolysis was obtained in the experimental setup discussed above. The inlet molar flow rate of RME and N_2 was kept constant at 1.15×10^{-4} and 2.5×10^{-3} mol/s, respectively. The temperature has been varied between 983 and 1063 K with 20 K increments. A detailed product distribution was obtained at each temperature and an overview can be found in Supporting Information. Figure 6 presents the GC×GC-FID chromatogram of the reactor effluent at 983 K. There is a clear connection between the position in the GC×GC-chromatogram of the esters, olefins, and aromatics based on the number of carbon atoms as observed earlier.[32] At the lowest temperature examined, that is, 983 K, the reactor effluent contains unconverted feed, note, however, that the

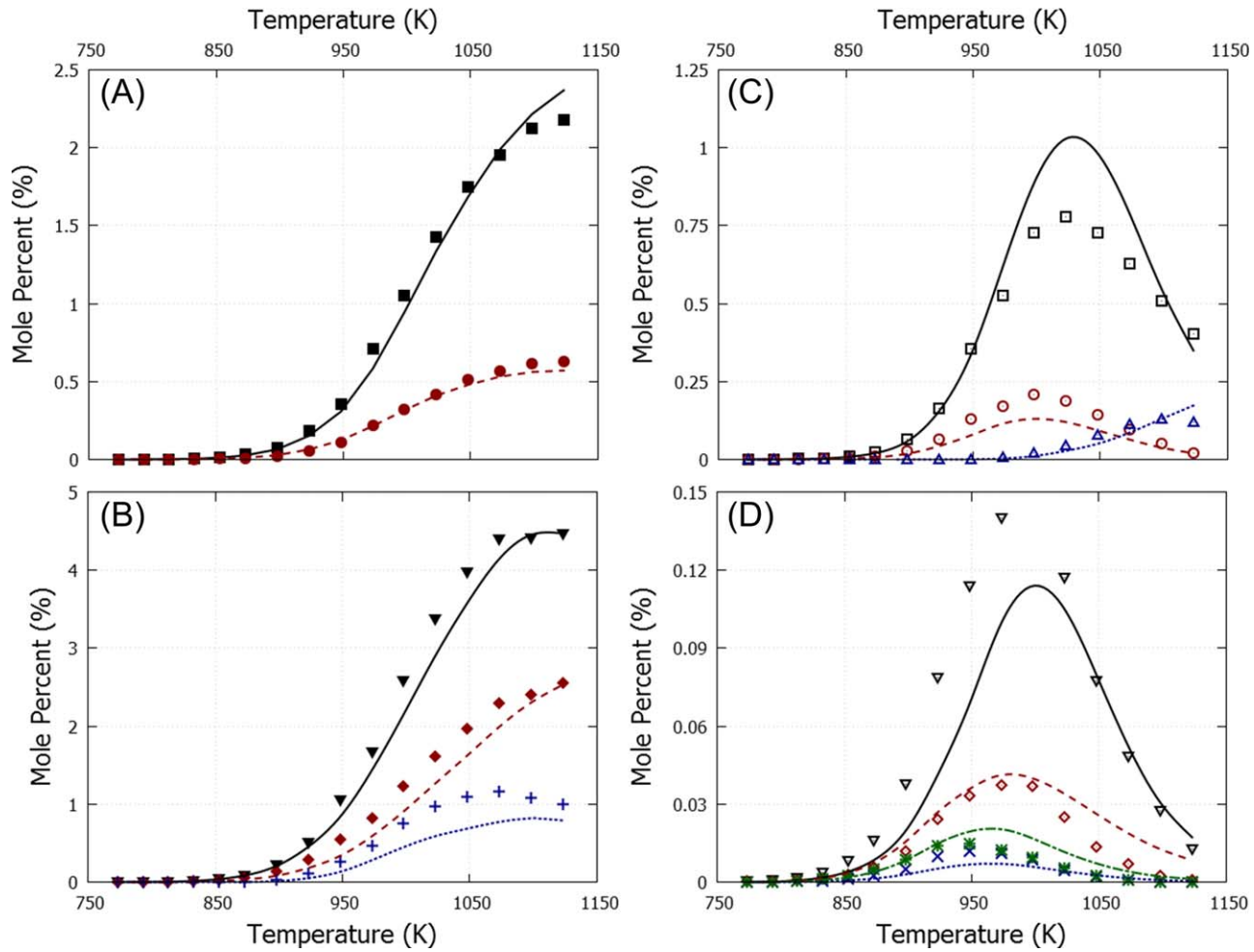

Figure 5. Mole fractions as a function of temperature for MD pyrolysis in a jet-stirred reactor[52]

(A) ■—CO, ●—CO_2; (B) ▼—C_2H_4, ◆—CH_4, +—1,3-butadiene (multiplied by 5); (C) □—C_3H_6, ○—1-butene, △—benzene; (D) ▽—methyl 2-propenoate, ◇—methyl 3-butenoate, ×—methyl 4-pentenoate, ✳—methyl 5-hexenoate; lines, calculated with CHEMKIN using the perfectly stirred reactor model and the developed kinetic model. [Color figure can be viewed in the online issue, which is available at wileyonlinelibrary.com.]

conversion already exceeds 95%, which is substantially higher than the conversion observed for MD pyrolysis at comparable operating conditions. Furthermore, a high fraction of aromatics was found at each temperature which differs from the MD pyrolysis effluent discussed earlier.

Kinetic Model. RME are typically composed of five major components. The major component of the examined RME mixture in this work is methyl oleate (C18:1). The presence of a C═C double bond in the alkyl chain implies that a difference in reactivity compared to MD can be expected. The C—C bond dissociation energy between an allylic and a secondary carbon atom is approximately 40 kJ/mol lower than between two secondary carbon atoms.[82] Consequently, C—C scission will be rather fast, leading to a relatively large radical pool explaining the high conversion observed experimentally, even at low temperatures. Besides hydrogen abstraction, small radicals can react with unsaturated methyl esters by addition onto the carbon double bond.

The primary decomposition products following hydrogen abstraction from methyl oleate are presented in Figure 7. Hydrogen can be abstracted from carbon atoms with label M, 2–8 and 11–18. Hydrogen abstraction from carbon atoms 9 and 10 is neglected due to the creation of unfavorable vinylic radicals. Decomposition of radicals close to the ester functionality causes formation of small oxygenated species such as $^{\bullet}$C(═O)OCH3, formaldehyde, and CO. Methyl oleate radicals with a radical center along the alkyl chain have similar decomposition routes. For example, methyl oleate radicals with a radical center on carbons atoms with label 11–16 can form an

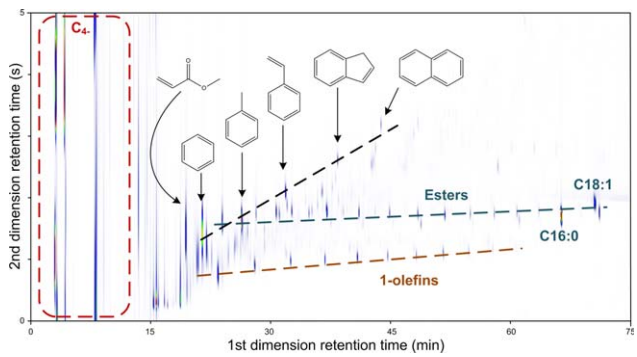

Figure 6. GC×GC-FID chromatogram of the rapeseed methyl ester (RME) pyrolysis effluent at $T = 983$ K, $P = 0.17$ MPa, $F_{RME} = 1.15 \times 10^{-4}$ mol/s and $F_{N2} = 2.5 \times 10^{-3}$ mol/s.

[Color figure can be viewed in the online issue, which is available at wileyonlinelibrary.com.]

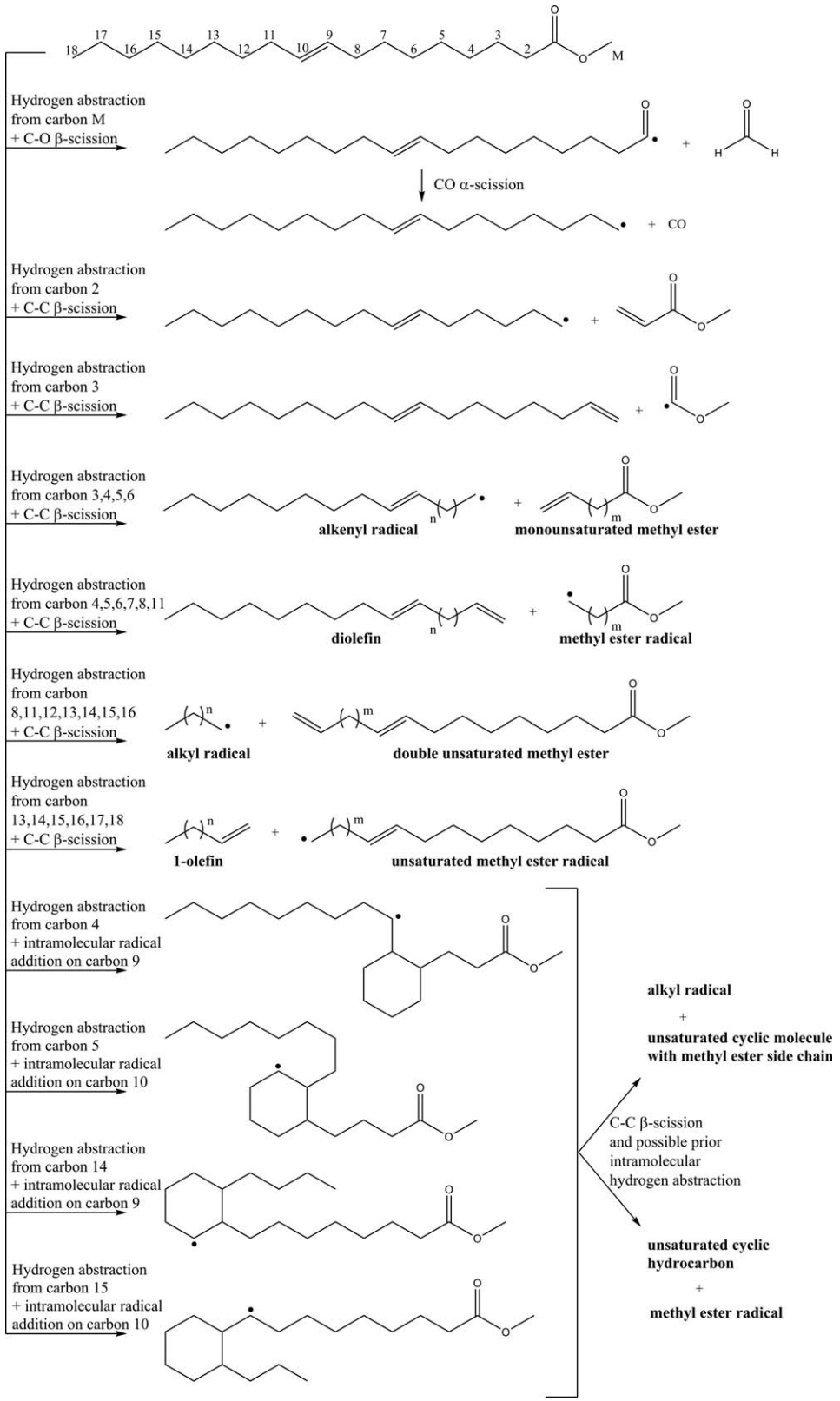

Figure 7. Reaction routes following hydrogen abstraction from methyl oleate.

alkyl radical and a double unsaturated methyl ester. Analogous reaction routes have been grouped to reduce the size of Figure 7. Single and double unsaturated esters and olefins are formed by decomposition of radicals along the alkyl chain by C—C β-scission. The presence of a double bond in methyl oleate enables intramolecular addition reactions. In this work, 5-membered and 6-membered intramolecular radical addition reactions, both endo and exo, are considered. For example, a methyl oleate radical with radical center on carbon 5 can form a monounsaturated methyl ester plus an alkenyl radical by C—C β-scission, a diolefin plus a methyl ester radical by C—C β-scission, or a cyclic methyl ester radical. Cyclic methyl ester

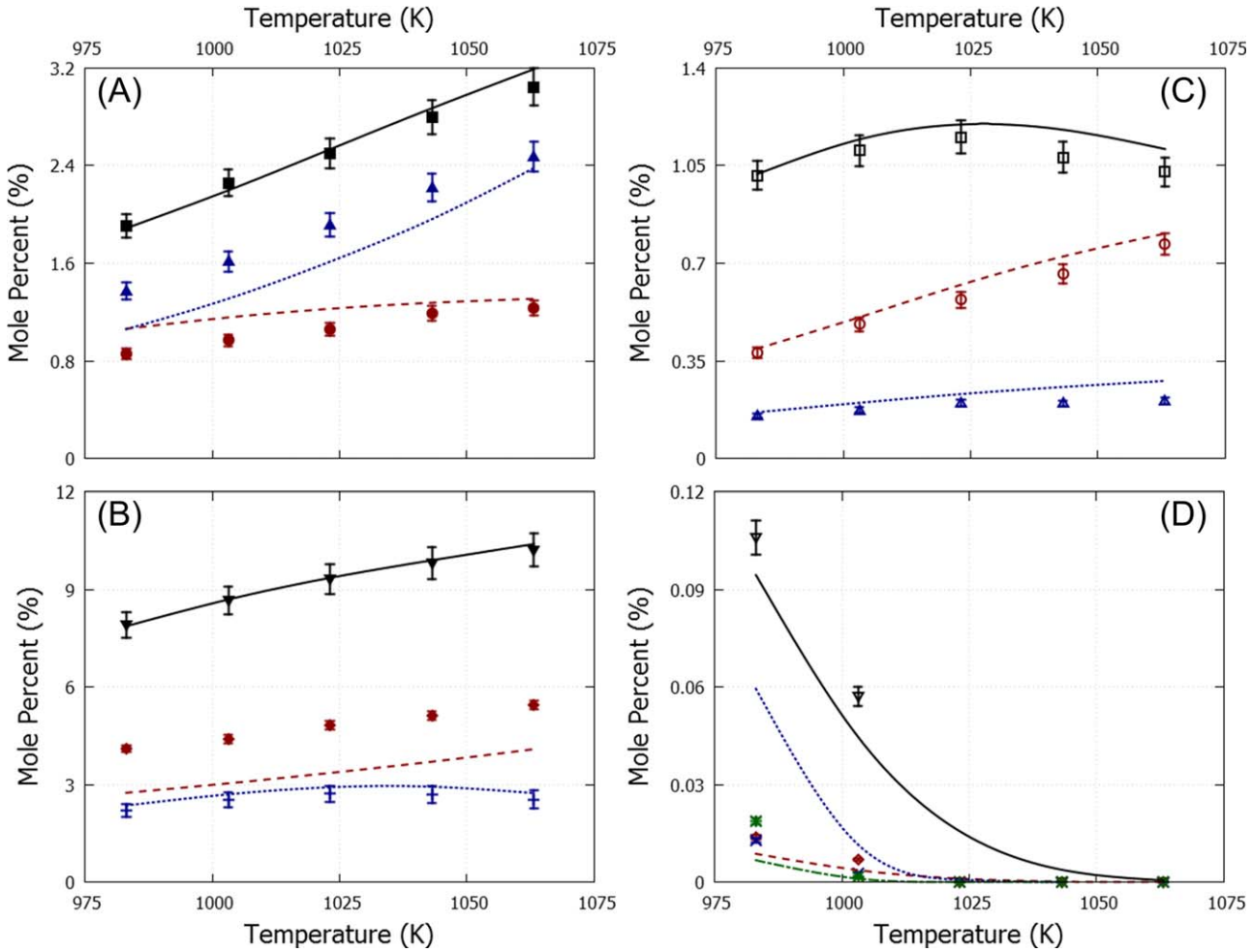

Figure 8. Mole fractions as a function of temperature for RME pyrolysis in a tubular reactor, $P = 0.17$ MPa, $F_{RME} = 1.15 \times 10^{-4}$ mol/s, $F_{N2} = 2.5 \times 10^{-3}$ mol/s: (A) ■—CO, ●—CO_2, ▲—H_2; (B) ▼—C_2H_4, ◆—CH_4, +—C_3H_6; (C) □—1,3-butadiene, ○—benzene, △—toluene; (D) ▽—methyl palmitate, ◇—methyl stearate, ×—methyl oleate, ✱—methyl linoleate; lines, mole fraction profiles calculated with CHEMKIN using the plug flow reactor model and the developed kinetic model.

[Color figure can be viewed in the online issue, which is available at wileyonlinelibrary.com.]

radicals can react by C—C β-scission, C—H β-scission and intramolecular hydrogen abstraction. A wide variety of unsaturated cyclic molecules can be formed. These molecules consist of a cyclic core with possible alkenyl, alkyl, and methyl ester side chains. This complex product spectrum is not presented in Figure 7, again to reduce the size of the picture, but is part of the developed kinetic model which can be found in Supporting Information.

The stoichiometric coefficients in the equivalent reaction for hydrogen abstraction from methyl oleate of double unsaturated methyl esters, respectively, diolefins, are approximately twice as large as those of monounsaturated methyl esters, respectively, 1-olefins. The former molecules are mainly formed through C—C β-scission of allylic radicals, the most abundantly formed radicals following hydrogen abstraction. Cyclic molecules which are formed following hydrogen abstraction from methyl oleate can be divided in two groups, cyclic molecules with a methyl ester functionality and cyclic molecules without a methyl ester functionality, see Figure 7. Both types of molecules have similar stoichiometric coefficients in the equivalent reaction for hydrogen abstraction from methyl oleate. These molecules are formed through similar intramolecular radical addition pathways starting from methyl oleate with a radical on carbon 4, 5, 15, or 16. The latter atoms are all secondary carbon atoms and, as such, the corresponding radicals have a similar formation rate.

Model performance. Experimental product mole fraction profiles for RME pyrolysis were obtained using the tubular reactor, discussed previously, while varying reactor temperature and keeping RME and N_2 molar flow rates fixed at 1.15×10^{-4} and 2.5×10^{-3} mol/s, respectively. The obtained experimental results are compared with calculated results using the developed kinetic model in Figures 8–10. Saggese et al.[83] developed a lumped kinetic model for the pyrolysis and combustion of biodiesel. Performance of their model can be found in Supporting Information. Calculated and experimental results for methyl palmitate (C16:0), methyl stearate (C18:0), methyl oleate (C18:1), and methyl linoleate (C18:2) are displayed in Figure 8D. Methyl linolenate (C18:3) was not detected in the reactor effluent. This is in line with model calculations which predict a mole percentage below 0.002 at 983 K, that is, the lowest temperature examined experimentally. Despite the feed being composed of over 50 mol % methyl oleate, methyl palmitate is the most abundant feed methyl ester remaining in the reactor effluent after pyrolysis at 983 K. As discussed earlier, the allylic carbon atoms in methyl

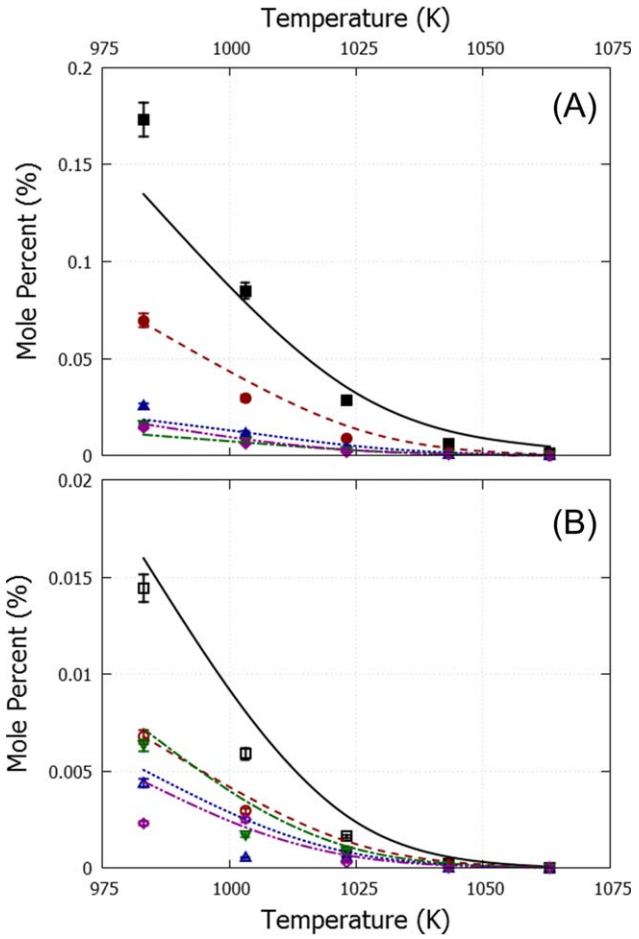

Figure 9. Mole fractions as a function of temperature for RME pyrolysis in a tubular reactor, $P = 0.17$ MPa, $F_{RME} = 1.15 \times 10^{-4}$ mol/s, $F_{N2} = 2.5 \times 10^{-3}$ mol/s: (A) ■—1-hexene, ●—1-heptene, ▲—1-octene, ▼—1-nonene, ◆—1-decene; (B) □—1-undecene, ▽—1-dodecene, ◇—1-tridecene, ○—1-tetradecene, —1-pentadecene; lines, mole fraction profiles calculated with CHEMKIN using the plug flow reactor model and the developed kinetic model.

[Color figure can be viewed in the online issue, which is available at wileyonlinelibrary.com.]

oleate enhance its reactivity with respect to hydrogen abstraction and scission reactions. Radical addition reactions on the carbon double bond are responsible for 10% of methyl oleate consumption at 1063 K.

Both CO and CO_2 are predicted well by the kinetic model, see Figure 8A. Only for CO_2, there is a small over prediction at the lowest investigated temperatures, that is, 983 K. The kinetic data applied for the decomposition of the ester functionality has been validated for MD pyrolysis earlier. The double bonds in the feed mixture are separated from the ester group by seven carbon atoms and, thus, their influence on the formation of carbon oxides can be expected to be negligible.

A high fraction of small olefins was observed which is in line with other works studying long carbon chain feedstocks.[84,85] The calculated mole fraction profiles of the most abundant olefins, that is, ethene, propene and 1,3-butadiene match the experimental results, see Figure 8B, C. The degree of unsaturation of the feedstock has an effect on the relative quantities of these olefins, which is most obvious for 1,3-butadiene. At 1063 K, the ratio of 1,3-butadiene to ethene is approximately 1:10 on a molar basis for RME pyrolysis. At comparable conditions for MD pyrolysis, that is, high temperature and conversion, the ratio of 1,3-butadiene to ethene was 1:30. Radicals of saturated molecules, such as MD, can decompose by successive C—C β-scissions forming a high number of ethene molecules and a small radical. The presence of a double bond in the alkyl chain can, however, disrupt this sequence of β-scission reactions leading to resonantly stabilized radicals. These have a lower reactivity compared to their paraffinic counterparts but will eventually isomerize or decompose to 1,3-butadiene.[86]

As can be observed from Figure 8C, a high yield for aromatics was obtained during RME pyrolysis. The kinetic model

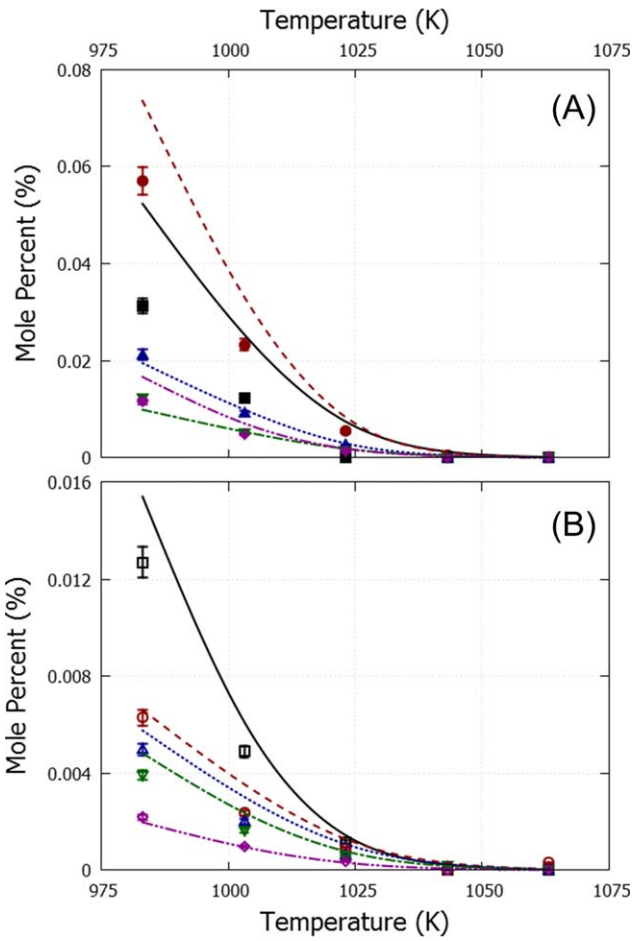

Figure 10. Mole fractions as a function of temperature for RME pyrolysis in a tubular reactor, $P = 0.17$ MPa, $F_{RME} = 1.15 \times 10^{-4}$ mol/s, $F_{N2} = 2.5 \times 10^{-3}$ mol/s: (A) ■—methyl hex-5-enoate, ●—methyl hept-6-enoate, ▲—methyl oct-7-enoate, ▼—methyl non-8-enoate, ◆—methyl dec-9-enoate; (B) □—methyl undec-10-enoate, △—methyl dodec-11-enoate, ▽—methyl tridec-12-enoate, ◇—methyl tetradec-13-enoate, ○—methyl pentadec-14-enoate; lines, mole fraction profiles calculated with CHEMKIN using the plug flow reactor model and the developed kinetic model.

[Color figure can be viewed in the online issue, which is available at wileyonlinelibrary.com.]

captures the temperature profile for benzene and toluene quite well. Benzene and toluene exhibit a linear trend compared to the exponential profile observed during MD pyrolysis. Especially at the lowest temperatures that were investigated experimentally, other reactions are expected to be dominant toward formation of aromatics compared to MD. The kinetic model predicts that the aromatic content for methyl oleate pyrolysis is a factor 10 higher compared to methyl stearate pyrolysis at 983 K and at similar conversion. This effect of a double bond has been observed before.[2,83,87–89]

As explained earlier, the double bond in unsaturated methyl esters, such as methyl oleate, enables intramolecular radical addition reactions. While it could be hypothesized that the formation of cyclic molecules in highly unsaturated moieties could occur through Diels Alder type reactions,[24] recent work showed that this path is of minor importance in thermal cracking of triglycerides compared to intramolecular radical addition.[87] Intramolecular radical addition competes with C—C β-scission for the decomposition of unsaturated methyl ester radicals. Comparison of the kinetic parameters of the reference reactions of both families, see Table 2, indicate that intramolecular radical addition will be dominant at low temperatures given its relatively low activation energy. At high temperatures, the C—C β-scission will become competitive but aromatics will start forming through other reaction paths such as propargyl recombination[90–92] (the C3 pathway), vinyl addition on 1,3-butadiene followed by cyclization[44,93] (the C4 pathway), and cyclopentadienyl-methyl recombination[46] (the C5 pathway). The linear increase in benzene and toluene yield as a function of temperature for RME can thus be considered as a consequence of intramolecular radical addition (especially at low temperature) complemented with the C3, C4, and C5 pathways. For esters with a saturated alkyl chain, only the latter three pathways contribute to formation of aromatics.

Figure 9 and 10 show the experimental and calculated mole fraction profiles of 1-olefins and monounsaturated methyl esters, respectively, with an alkyl chain varying between 6 and 15 carbon atoms, as a function of temperature. All displayed molecules have a low yield in the investigated operating range and exhibit a monotonic decreasing trend with an approximate zero mole percentage at the highest temperature, that is, 1063 K. Previous works that focused on maximizing the yield of these components[3,94] were performed in a lower temperature range, that is, between 600 (high residence time) and 900 K (low residence time). The mole fraction profiles are captured accurately by the kinetic model, both quantitatively and qualitatively.

Conclusions

A detailed kinetic model for the pyrolysis of MD and RME is presented. All reaction rate coefficients are systematically calculated using a comprehensive group additive method. Analysis of the kinetic model shows that the μ-hypothesis and PSSA are valid for all radicals with six or more carbon atoms, independent of the presence of oxygen. The concentrations of these heavy radicals can be eliminated from the model equations, which allow to come up with equivalent single-step reactions for the decomposition of heavy methyl esters. This also reduces the complexity of the kinetic network substantially, without loss of accuracy. The stoichiometric coefficients of these reactions depend on temperature. In the investigated operating range, neglecting this temperature dependence only has a minor effect on model predictions. Existing and new experimental data for the thermal decomposition of MD and RME showed an excellent agreement with model calculations without any adjustment of the reaction rate coefficients. This shows the huge potential of the used approach for modeling the decomposition of other hetero atom containing compound classes.

The ester function has an effect on the reactivity of the neighboring carbon atoms and accurate kinetic data is required to properly predict the formation of small oxygenated species. Most of the dominant elementary reaction families, such as intermolecular/intramolecular hydrogen abstraction and β-scission, occur on the alkyl chain and group additive values originally obtained for pure hydrocarbons are shown to be valid. Intramolecular radical addition onto the C=C double bond present in RME are important under the studied conditions. The resulting cyclic intermediates are precursors for aromatics.

Acknowledgments

The authors acknowledge financial support from the Long Term Structural Methusalem Funding by the Flemish Government and the Research Board of Ghent University (BOF).

Notation

Roman

A = pre-exponential factor, m^3/(mol s) or/s
$\tilde{A}$ = single-event pre-exponential factor, m^3/(mol s) or/s
$\tilde{A}_{ref}$ = single-event pre-exponential factor of the reference reaction, m^3/(mol s) or 1/s
c_j = concentration of species j, mol/m^3
Δc_j^s = instantaneous error on c_j when applying the PSSA, mol/m^3
CX:Y = methyl ester with a carbon chain of length X with Y double bond
d_t = internal tube diameter, m
E_a = activation energy, kJ/mol
$E_{a,ref}$ = activation energy of the reference reaction, kJ/mol
FID = flame ionization detector
F_j^0 = inlet molar flow rate of species j, mol/s
$\Delta GAV_{\tilde{A}}^0$ = pre-exponential group additive value relative to the reference reaction, m^3/(mol s) or/s
$\Delta GAV_{E_a}^0$ = activation energy group additive value relative to the reference reaction, kJ/mol
GC×GC = two dimensional gas chromatograph
k = rate coefficient, m^3/(mol s) or 1/s
n_e = number of single events
P = pressure, MPa
PAH = polycyclic aromatic hydrocarbon
PSSA = pseudosteady-state approximation
r_j = rate of reaction j, mol/(m^3 s)
RME = rapeseed methyl esters
T = temperature, K
TCD = thermal conductivity detector
TOF-MS = time of flight mass spectrometer
$v_{i,j}$ = stoichiometric coefficient of species i with respect to reaction j
z = axial position

Greek

$\alpha_j(T)$ = = stoichiometric coefficient of species j in a single-step equivalent reaction, obtained after elimination of the concentration of μ-radicals using the PSSA, at temperature T

Literature Cited

1. Dente M, Bozzano G, Faravelli T, Marongiu A, Pierucci S, Ranzi E. Kinetic modelling of pyrolysis processes in gas and condensed phase. *Adv Chem Eng*. 2007;32:51–166.
2. Billaud F, Dominguez V, Broutin P, Busson C. Production of hydrocarbons by pyrolysis of methyl esters from rapeseed oil. *J Am Oil Chem Soc*. 1995;72:1149–1154.
3. Archambault D, Billaud F. Experimental and modelling study of methyl oleate pyrolysis between 500 and 650°C. *J Chim Phys PCB*. 1999;96:778–796.

4. Vandewiele NM, Van Geem KM, Reyniers M-F, Marin GB. Genesys: kinetic model construction using chemo-informatics. *Chem Eng J*. 2012;207:526–538.
5. Rangarajan S, Bhan A, Daoutidis P. Rule-based generation of thermochemical routes to biomass conversion. *Ind Eng Chem Res*. 2010; 49:10459–10470.
6. Van Geem KM, Reyniers M-F, Marin GB, Song J, Green WH, Matheu DM. Automatic reaction network generation using RMG for steam cracking of n-hexane. *AlChE J*. 2006;52:718–730.
7. Buda F, Bounaceur R, Warth V, Glaude PA, Fournet R, Battin-Leclerc F. Progress toward a unified detailed kinetic model for the autoignition of alkanes from C4 to C10 between 600 and 1200 K. *Combust Flame*. 2005;142:170–186.
8. Broadbelt LJ, Stark SM, Klein MT. Computer-generated pyrolysis modeling – on-the-fly generation of species, reactions, and rates. *Ind Eng Chem Res*. 1994;33:790–799.
9. De Witt MJ, Dooling DJ, Broadbelt LJ. Computer generation of reaction mechanisms using quantitative rate information: application to long-chain hydrocarbon pyrolysis. *Ind Eng Chem Res*. 2000;39: 2228–2237.
10. Moreac G, Blurock ES, Mauss F. Automatic generation of a detailed mechanism for the oxidation of n-decane. *Combust Sci Technol*. 2006;178:2025–2038.
11. Benson SW. Thermochemical Kinetics: Methods for the Estimation of Thermochemical Data and Rate Parameters. New York: Wiley, 1976.
12. Broadbelt LJ, Pfaendtner J. Lexicography of kinetic modeling of complex reaction networks. *AlChE J*. 2005;51:2112–2121.
13. Clymans PJ, Froment GF. Computer generation of the reaction paths and rate equations in the thermal cracking of normal and branched paraffins. *Comput Chem Eng*. 1984;8:137–142.
14. Graboski MS, McCormick RL. Combustion of fat and vegetable oil derived fuels in diesel engines. *Prog Energy Combust Sci*. 1998;24: 125–164.
15. Schönborn A, Ladommatos N, Williams J, Allan R, Rogerson J. The influence of molecular structure of fatty acid monoalkyl esters on diesel combustion. *Combust Flame*. 2009;156:1396–1412.
16. Menkiel B, Donkerbroek A, Uitz R, Cracknell R, Ganippa L. Combustion and soot processes of diesel and rapeseed methyl ester in an optical diesel engine. *Fuel*. 2014;118:406–415.
17. Garner S, Brezinsky K. Biologically derived diesel fuel and NO formation: an experimental and chemical kinetic study, Part 1. *Combust Flame*. 2011;158:2289–2301.
18. Sun J, Caton JA, Jacobs TJ. Oxides of nitrogen emissions from biodiesel-fuelled diesel engines. *Prog Energy Combust Sci*. 2010;36: 677–695.
19. Palash SM, Kalam MA, Masjuki HH, Masum BM, Rizwanul Fattah IM, Mofijur M. Impacts of biodiesel combustion on NOx emissions and their reduction approaches. *Renew Sust Energ Rev*. 2013;23: 473–490.
20. Ma F, Hanna MA. Biodiesel production: a review. *Bioresour Technol*. 1999;70:1–15.
21. Balaji G, Cheralathan M. Potential of various sources for biodiesel production. *Energ Source Part A*. 2013;35:831–839.
22. Zamostny P, Belohlav Z, Smidrkal J. Production of olefins via steam cracking of vegetable oils. *Resour Conserv Recycl*. 2012;59:47–51.
23. Šmidrkal J, Belohlav Z, Zámostný P, Filip V. Olefin production through pyrolysis of triacylglycerols. *Lipid Technol*. 2009;21:220–223.
24. Maher KD, Bressler DC. Pyrolysis of triglyceride materials for the production of renewable fuels and chemicals. *Bioresour Technol*. 2007;98:2351–2368.
25. Pyl SP, Schietekat CM, Reyniers M-F, Abhari R, Marin GB, Van Geem KM. Biomass to olefins: cracking of renewable naphtha. *Chem Eng J*. 2011;176-177:178–187.
26. Laidler KJ. *Chemical Kinetics*. New York: Harper & Row, 1987.
27. Turanyi T, Tomlin AS, Pilling MJ. On the error of the quasi-steady-state approximation. *J Phys Chem-US*. 1993;97:163–172.
28. Gusmão GS, Christopher P. A general and robust approach for defining and solving microkinetic catalytic systems. *AlChE J*. 2015;61:188–199.
29. Marin GB, Yablonsky GS. *Kinetics of Chemical Reactions*. New York: Wiley, 2011.
30. Harper MR, Van Geem KM, Pyl SP, Marin GB, Green WH. Comprehensive reaction mechanism for n-butanol pyrolysis and combustion. *Combust Flame*. 2011;158:16–41.
31. Djokic M, Carstensen HH, Van Geem KM, Marin GB. The thermal decomposition of 2,5-dimethylfuran. *Proc Combust Inst*. 2013;34: 251–258.
32. Pyl SP, Schietekat CM, Van Geem KM, Reyniers M-F, Vercammen J, Beens J, Marin GB. Rapeseed oil methyl ester pyrolysis: on-line product analysis using comprehensive two-dimensional gas chromatography. *J Chromatogr A*. 2011;1218:3217–3223.
33. Cargill. Available at: http://www.cargill.be/en/products/grain-oilseeds/biodiesel/. Accessed 16 July 2015.
34. Van Geem KM, Reyniers M-F, Marin GB. Challenges of modeling steam cracking of heavy feedstocks. *Oil Gas Sci Technol*. 2008;63: 79–94.
35. Fake DM, Nigam A, Klein MT. Mechanism based lumping of pyrolysis reactions: lumping by reactive intermediates. *Appl Catal A-Gen*. 1997;160:191–221.
36. Hillewaert LP, Dierickx JL, Froment GF. Computer-generation of reaction schemes and rate-equations for thermal-cracking. *AlChE J*. 1988;34:17–24.
37. Dente M, Ranzi E, Goossens AG. Detailed prediction of olefin yields from hydrocarbon pyrolysis through a fundamental simulation program SPYRO. *Comput Chem Eng*. 1979;3:61–75.
38. De Bruycker R, Anthonykutty JM, Linnekoski J, Harlin A, Lehtonen J, Van Geem KM, Räsänen J, Marin GB. Assessing the potential of crude tall oil for the production of green-base chemicals: an experimental and kinetic modeling study. *Ind Eng Chem Res*. 2014;53: 18430–18442.
39. Ranzi E, Dente M, Goldaniga A, Bozzano G, Faravelli T. Lumping procedures in detailed kinetic modeling of gasification, pyrolysis, partial oxidation and combustion of hydrocarbon mixtures. *Prog Energy Combust Sci*. 2001;27:99–139.
40. Huynh LK, Violi A. Thermal decomposition of methyl butanoate: ab initio study of a biodiesel fuel surrogate. *J Org Chem*. 2008;73:94–101.
41. Huynh LK, Lin KC, Violi A. Kinetic modeling of methyl butanoate in shock tube. *J Phys Chem A*. 2008;112:13470–13480.
42. Farooq A, Davidson DF, Hanson RK, Huynh LK, Violi A. An experimental and computational study of methyl ester decomposition pathways using shock tubes. *Proc Combust Inst*. 2009;32:247–253.
43. Farooq A, Ren W, Lam KY, Davidson DF, Hanson RK, Westbrook CK. Shock tube studies of methyl butanoate pyrolysis with relevance to biodiesel. *Combust Flame*. 2012;159:3235–3241.
44. Sabbe MK, Van Geem KM, Reyniers M-F, Marin GB. First principle-based simulation of ethane steam cracking. *AlChE J*. 2011;57:482–496.
45. Li J, Zhao ZW, Kazakov A, Chaos M, Dryer FL, Scire JJ. A comprehensive kinetic mechanism for CO, CH_2O, and CH_3OH combustion. *Int J Chem Kinet*. 2007;39:109–136.
46. Cavallotti C, Polino D, Frassoldati A, Ranzi E. Analysis of some reaction pathways active during cyclopentadiene pyrolysis. *J Phys Chem A*. 2012;116:3313–3324.
47. Cavallotti C, Polino D. On the kinetics of the C5H5 + C5H5 reaction. *Proc Combust Inst*. 2013;34:557–564.
48. Ranzi E, Dente M, Plerucci S, Biardi G. Initial product distributions from pyrolysis of normal and branched paraffins. *Ind Eng Chem Fund*. 1983;22:132–139.
49. Schietekat CM, van Goethem MWM, Van Geem KM, Marin GB. Swirl flow tube reactor technology: an experimental and computational fluid dynamics study. *Chem Eng J*. 2014;238:56–65.
50. Zhang Y, Qian F, Schietekat CM, Van Geem KM, Marin GB. Impact of flue gas radiative properties and burner geometry in furnace simulations. *AlChE J*. 2015;61:936–954. DOI:10.1002/aic.14724.
51. Fisher EM, Pitz WJ, Curran HJ, Westbrook CK. Detailed chemical kinetic mechanisms for combustion of oxygenated fuels. *Proc Combust Inst*. 2000;28:1579–1586.
52. Herbinet O, Glaude P-A, Warth V, Battin-Leclerc F. Experimental and modeling study of the thermal decomposition of methyl decanoate. *Combust Flame*. 2011;158:1288–1300.
53. Pyl SP, Van Geem KM, Puimège P, Sabbe MK, Reyniers M-F, Marin GB. A comprehensive study of methyl decanoate pyrolysis. *Energy*. 2012;43:146–160.
54. Mehl M, Vanhove G, Pitz WJ, Ranzi E. Oxidation and combustion of the n-hexene isomers: a wide range kinetic modeling study. *Combust Flame*. 2008;155:756–772.
55. Harding LB, Georgievskii Y, Klippenstein SJ. Predictive theory for hydrogen atom - hydrocarbon radical association kinetics. *J Phys Chem A*. 2005;109:4646–4656.
56. Harding LB, Klippenstein SJ, Georgievskii Y. On the combination reactions of hydrogen atoms with resonance-stabilized hydrocarbon radicals. *J Phys Chem A*. 2007;111:3789–3801.
57. Sabbe MK, Vandeputte A, Reyniers M-F, Waroquier M, Marin GB. Modeling the influence of resonance stabilization on the kinetics of hydrogen abstractions. *Phys Chem Chem Phys*. 2010;12:1278–1298.

58. Paraskevas PD, Sabbe MK, Reyniers M-F, Papayannakos NG, Marin GB. Kinetic modeling of α-hydrogen abstractions from unsaturated and saturated oxygenate compounds by carbon-centered radicals. *ChemPhysChem*. 2014;15:1849–1866.
59. Paraskevas PD, Sabbe MK, Reyniers M-F, Papayannakos NG, Marin GB. Kinetic modeling of α-hydrogen abstractions from unsaturated and saturated oxygenate compounds by hydrogen atoms. *J Phys Chem A*. 2014;118:9296–9309.
60. Sabbe MK, Reyniers M-F, Van Speybroeck V, Waroquier M, Marin GB. Carbon-centered radical addition and beta-scission reactions: modeling of activation energies and pre-exponential factors. *ChemPhysChem*. 2008;9:124–140.
61. Sabbe MK, Reyniers M-F, Waroquier M, Marin GB. Hydrogen radical additions to unsaturated hydrocarbons and the reverse beta-scission reactions: modeling of activation energies and pre-exponential factors. *ChemPhysChem*. 2010;11:195–210.
62. Sabbe MK, Vandeputte A, Reyniers M-F, Van Speybroeck V, Waroquier M, Marin GB. Ab initio thermochemistry and kinetics for carbon-centered radical addition and beta-scission reactions. *J Phys Chem A*. 2007;111:8416–8428.
63. Metcalfe WK, Dooley S, Curran HJ, Simmie JM, El-Nahas AM, Navarro MV. Experimental and modeling study of $C_5H_{10}O_2$ ethyl and methyl esters. *J Phys Chem A*. 2007;111:4001–4014.
64. Watanabe M, Tsukagoshi M, Hirakoso H, Adschiri T, Arai K. Kinetics and product distribution of n-hexadecane pyrolysis. *AlChE J*. 2000;46:843–856.
65. El-Nahas AM, Navarro MV, Simmie JM, Bozzelli JW, Curran HJ, Dooley S, Metcalfe W. Enthalpies of formation, bond dissociation energies and reaction paths for the decomposition of model biofuels: ethyl propanoate and methyl butanoate. *J Phys Chem A*. 2007;111:3727–3739.
66. Curran HJ. Rate constant estimation for C-1 to C-4 alkyl and alkoxyl radical decomposition. *Int J Chem Kinet*. 2006;38:250–275.
67. Turanyi T. Applications of sensitivity analysis to combustion chemistry. *Reliab Eng Syst Saf*. 1997;57:41–48.
68. Fournet R, Warth V, Glaude PA, Battin-Leclerc F, Scacchi G, Côme GM. Automatic reduction of detailed mechanisms of combustion of alkanes by chemical lumping. *Int J Chem Kinet*. 2000;32:36–51.
69. Dijkmans T, Schietekat CM, Van Geem KM, Marin GB. GPU based simulation of reactive mixtures with detailed chemistry in combination with tabulation and an analytical Jacobian. *Comput Chem Eng*. 2014;71:521–531.
70. Kovacs T, Zsely IG, Kramarics A, Turanyi T. Kinetic analysis of mechanisms of complex pyrolytic reactions. *J Anal Appl Pyrolysis*. 2007;79:252–258.
71. Saeys M, Reyniers M-F, Marin GB, Van Speybroeck V, Waroquier M. Ab initio group contribution method for activation energies for radical additions. *AlChE J*. 2004;50:426–444.
72. Muller C, Michel V, Scacchi G, Come GM. THERGAS - a computer program for the evaluation of thermochemical data of molecules and free-radicals in the gas-phase. *J Chim Phys PCB*. 1995;92:1154–1178.
73. Green WH, Allen JW, Bhoorasingh P, Buesser BA, Ashcraft RW, Beran GJ, Class CA, Gao C, Goldsmith CF, Harper MR, Jalan A, Khanshan FS, Magoon GR, Matheu DM, Merchant SS, Mo JD, Petway S, Raman S, Sharma S, Slakman B, Song J, Van Geem KM, Wen J, West RH, Wong A, Wong H-W, Yelvington PE, Yee N, J. Y. Reaction Mechanism Generator. 2013; Available at: http://rmg.mit.edu/. Accessed 16 July 2015.
74. Sabbe MK, De Vleeschouwer F, Reyniers M-F, Waroquier M, Marin GB. First principles based group additive values for the gas phase standard entropy and heat capacity of hydrocarbons and hydrocarbon radicals. *J Phys Chem A*. 2008;112:12235–12251.
75. Paraskevas PD, Sabbe MK, Reyniers M-F, Papayannakos NG, Marin GB. Group additive values for the gas-phase standard enthalpy of formation, entropy and heat capacity of oxygenates. *Chem-Eur J*. 2013;19:16431–16452.
76. *CHEMKIN-PRO [computer program]. Version 15101*. San Diego, CA: Reaction Design, Inc.; 2010.
77. Cuoci A, Frassoldati A, Faravelli T, Ranzi E. OpenSMOKE++: an object-oriented framework for the numerical modeling of reactive systems with detailed kinetic mechanisms. *Comput Phys Commun*. 2015;192:237–264. DOI:10.1016/j.cpc.2015.1002.1014.
78. Grana R, Frassoldati A, Saggese C, Faravelli T, Ranzi E. A wide range kinetic modeling study of pyrolysis and oxidation of methyl butanoate and methyl decanoate – Note II: lumped kinetic model of decomposition and combustion of methyl esters up to methyl decanoate. *Combust Flame*. 2012;159:2280–2294.
79. Dievart P, Won SH, Dooley S, Dryer FL, Ju YG. A kinetic model for methyl decanoate combustion. *Combust Flame*. 2012;159:1793–1805.
80. Sarathy SM, Thomson MJ, Pitz WJ, Lu T. An experimental and kinetic modeling study of methyl decanoate combustion. *Proc Combust Inst*. 2011;33:399–405.
81. Farooq A, Davidson DF, Hanson RK, Westbrook CK. A comparative study of the chemical kinetics of methyl and ethyl propanoate. *Fuel*. 2014;134:26–38.
82. Luo Y. Handbook of Bond Dissociation Energies in Organic Compounds. Boca Raton, FL: CRC Press, 2002.
83. Saggese C, Frassoldati A, Cuoci A, Faravelli T, Ranzi E. A lumped approach to the kinetic modeling of pyrolysis and combustion of biodiesel fuels. *Proc Combust Inst*. 2013;34:427–434.
84. Pyl SP, Dijkmans T, Antonykutty JM, Reyniers M-F, Harlin A, Van Geem KM, Marin GB. Wood-derived olefins by steam cracking of hydrodeoxygenated tall oils. *Bioresour Technol*. 2012;126:48–55.
85. Herbinet O, Marquaire PM, Battin-Leclerc F, Fournet R. Thermal decomposition of n-dodecane: experiments and kinetic modeling. *J Anal Appl Pyrolysis*. 2007;78:419–429.
86. Zhang K, Togbé C, Dayma G, Dagaut P. Experimental and kinetic modeling study of trans-methyl-3-hexenoate oxidation in JSR and the role of CC double bond. *Combust Flame*. 2014;161:818–825.
87. Kubatova A, St'avova J, Seames WS, Luo Y, Sadrameli SM, Linnen MJ, Baglayeva GV, Smoliakova IP, Kozliak EI. Triacylglyceride thermal cracking: pathways to cyclic hydrocarbons. *Energ Fuel*. 2012;26:672–685.
88. Fridlyand A, Goldsborough SS, Brezinsky K, Merchant SS, Green WH. Influence of the double bond position on the oxidation of decene isomers at high pressures and temperatures. *Proc Combust Inst*. 2015;35:333–340.
89. Sarathy SM, Gail S, Syed SA, Thomson MJ, Dagaut P. A comparison of saturated and unsaturated C-4 fatty acid methyl esters in an opposed flow diffusion flame and a jet stirred reactor. *Proc Combust Inst*. 2007;31:1015–1022.
90. Matheu DM, Grenda JM. A systematically generated, pressure-dependent mechanism for high-conversion ethane pyrolysis. 1. Pathways to the minor products. *J Phys Chem A*. 2005;109:5332–5342.
91. Hansen N, Miller JA, Westmoreland PR, Kasper T, Kohse-Höinghaus K, Wang J, Cool TA. Isomer-specific combustion chemistry in allene and propyne flames. *Combust Flame*. 2009;156:2153–2164.
92. Marchal C, Delfau J-L, Vovelle C, Moréac G, Mounaïm-Rousselle C, Mauss F. Modelling of aromatics and soot formation from large fuel molecules. *Proc Combust Inst*. 2009;32:753–759.
93. Cavallotti C, Rota R, Carrà S. Quantum chemistry computation of rate constants for reactions involved in the first aromatic ring formation. *J Phys Chem A*. 2002;106:7769–7778.
94. Seames W, Luo Y, Ahmed I, Aulich T, Kubatova A, Stavova J, Kozliak E. The thermal cracking of canola and soybean methyl esters: improvement of cold flow properties. *Biomass Bioenerg*. 2010;34:939–946.

Manuscript received Jan. 22, 2015, and revision received Apr. 11, 2015.